GA–A26173

# EDGE TURBULENCE AND SOL TRANSPORT IN TOKAMAKS

by

J.A. BOEDO

FEBRUARY 2009

GENERAL ATOMICS

# DISCLAIMER

GA–A26173

# EDGE TURBULENCE AND SOL TRANSPORT IN TOKAMAKS

by

J.A. BOEDO*

This is a preprint of a Review paper presented at the Eighteenth International Conference on Plasma Surface Interactions, May 26-30, 2008, in Toledo, Spain, and to be published in *J. Nucl. Mater.*

*University of California-San Diego, La Jolla, California.

Work supported in part by
the U.S. Department of Energy
under DE-FG02-07ER54917 and DE-FC02-04ER54698

GENERAL ATOMICS ATOMICS PROJECT 30200
FEBRUARY 2009

GENERAL ATOMICS

# ABSTRACT

Some key topics in tokamak edge plasma transport and turbulence are reviewed. Multi-device results reveal a new paradigm of scrape-off layer (SOL) transport. Radial transport is driven by intermittency throughout the SOL, in between edge localized modes (ELMs) in H-mode, and comprised of plasma filaments that are generated near the last closed flux surface likely by interchange instability. The filaments travel radially at speeds of ~1 km/s into the SOL and have a poloidal size of 1-3 cm in most devices. The radial transport in the SOL is poloidally asymmetric, by factors of 2-5, causing a pressure peak in the low field side. This asymmetry and other neo-classical terms, such as Pfirsch-Schlüter currents, are found to drive strong SOL flows. The intermittent particle flux is 20% of the total, including ELMs, at low collisionality, becoming 70% of total at high collisionality. Numerical and analytical models can reproduce the scaling of intermittency with collisionality as well as many details of the filament dynamics in the SOL.

# 1. INTRODUCTION

Knowledge of the edge/SOL plasma in toroidal devices is crucial because: (1) it is the boundary condition for the core plasma and thus the processes determining its properties are fundamental for the whole discharge, (2) determines the flow of particles and energy, and thus their removal from the plasma, to the plasma facing components, and (3) mediates the transport of impurities and helium ash between the walls and core, which affects discharge performance.

There are two important components in the edge/boundary transport, one is the radial transport across the last closed flux surface (LCFS) and in the scrape-off layer (SOL) and the other is the combination of poloidal and parallel transport that redistributes heat and particles in the SOL. The strength and distribution of these transport vehicles determine the location and strength of the heat and particle flux to the wall, the processes of recycling, impurity production/influx and helium ash removal. The shear layer near the LCFS creates the transport barrier of the high confinement mode (H-mode) and the height of the pedestal determines core parameters.

High performance tokamak discharges exhibit pulses of energy and particles (ELMs) that result on a transient heat/particle load on the wall/divertor components and therefore ELMs are one of ITER main concerns regarding lifetime of components and viability. A variety of techniques are being developed to suppress and/or ameliorate the effect of ELMs however, the inter-ELM and ELM-free plasma regimes still exhibit fast energy and particle radial transport, The edge radial transport is turbulence-dominated, as described in various reviews [1–8], ballooning in character and containing coherent filamentary structures that move convectively across magnetic surfaces. This ballooning, convective radial transport interacts with the parallel Pfirsch-Schlüter (PS) mechanism and classical drifts, sinks and sources to create the SOL transport. This paper reviews some recent results and understanding on cross-field (including ELMs) and parallel transport in the SOL and their interplay.

# 2. TURBULENT RADIAL TRANSPORT

Edge turbulence consists of density (n), potential (ϕ), temperature ($T_e$) and magnetic ($B_r$) fluctuations with normalized levels that increase away from the LCFS into the SOL and in a frequency range $f \sim$ 10 kHz–1 MHz featuring a broad spectrum with an autocorrelation time $t_c \sim$ 2–20 μs. The turbulence has a small spatial scale (~0.1–10 cm) in the cross-field plane but many meters along the magnetic field, like filaments. Many digital signal processing techniques [1–8] exist for turbulence and transport analysis [9], many developed for measurements with probes, which were the earliest turbulence diagnostics and can be arranged in arrays with varied geometry to produce a wide array of measurements [9–25].

## 2.1. PARTICLE FLUXES

Radial profiles of averaged and turbulent parameters measured with a fast probe [26] in the edge of the DIII-D tokamak are shown in Fig. 1(a)–(e) for L- and H-mode. The fluctuations are often larger (2x) across the SOL in L-mode. The relative electron density fluctuations at the outboard midplane generally increase [Fig. 1(c)] from $\partial n/n \sim 20\%$ to $\partial n/n \sim 100\%$ in the far SOL, increasing monotonically with radius across the last closed magnetic surface. Similar results are seen in other toroidal devices such as the TFTR tokamak, the ATF stellarator and the RFX RFP [27]. The plasma potential fluctuation level normalized to $T_e$ [Fig. 1(d)] has a similar magnitude to $\partial n/n$, but as seen in TEXT and in RFX [28], $\delta\phi/T_e < \tilde{n}/n$, so it does not always follow the Boltzmann relation indicating the effects of collisions, resistivity, electron inertia, viscosity or neutral interaction are at play. Electron temperature fluctuations fulfill $\delta T_e/T_e \sim$ (0.3–0.4) $\partial n/n$, as seen in TEXT, DIII-D, SINP, FTU and JET [29–33]. Broadband edge magnetic turbulence in tokamaks and stellarators, typically $\delta Br/B_T \sim 10^{-4}$ to $10^{-5}$ [34,35], is calculated to have negligible effect on transport. There is a clear difference between the "near-SOL", defined as $R - R_{sep} \leqq 2\%$ of minor radius (often 1-3 cm), where gradients are strong and plasma parameters vary over orders of magnitude, and the "far-SOL", further towards the wall [36,37], with nearly flat average gradients. Edge turbulence in tokamaks and stellarators has a spectrum-averaged poloidal correlation length $L_{pol} \sim$ 0.5–5 cm and a radial correlation length $L_{rad} \sim$ (0.5–1) $L_{pol}$. The parallel structure of the edge turbulence along $B$ has been measured with Langmuir probes indicating $L_{||} >> L_{\perp}$ [38,39] and is seen in the filamentary structure of edge light emission [40–42] as expected due to the rapid electron motion along $B$. The radial electrostatic particle flux, calculated from the density and potential signals [Eq. (1)], depends not only on density or electric field fluctuations, but the phase between them:

$$\tilde{\Gamma}_r = \frac{\left\langle \tilde{E}_\theta \tilde{n} \right\rangle}{B_\varphi} \quad . \tag{1}$$

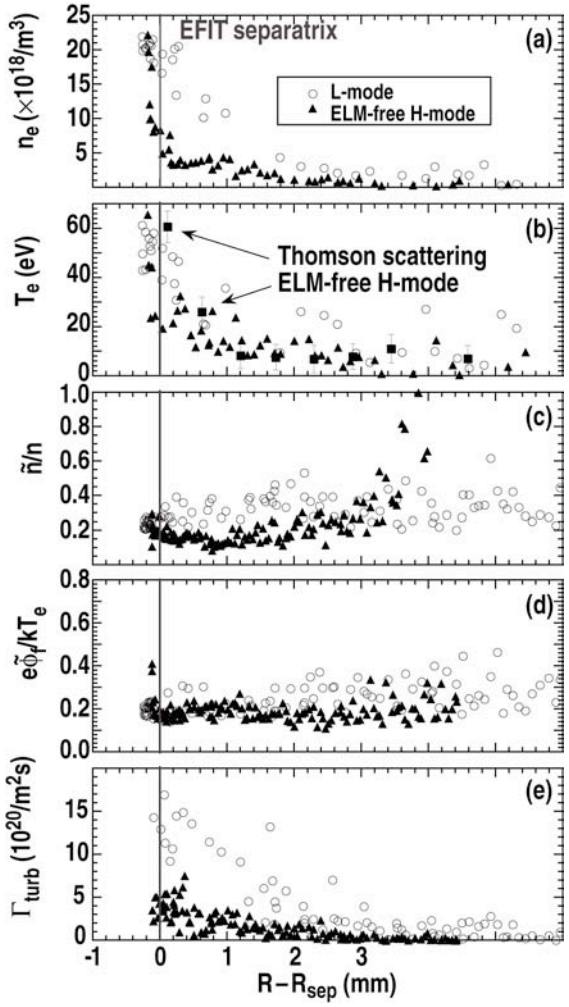


Fig. 1. Radial profiles in L-mode (open symbols) and H-mode (full symbols) DIII-D plasmas of: (a) density, (b) temperature, (c) normalized density fluctuations, (d) normalized potential fluctuations and (e) electrostatic turbulent particle flux. Squares in (b) show Thomson scattering measurements.

This $E \times B$ particle flux, shown in Fig. 1(e), is much larger (3x) in the L-mode than in H-mode [26], and has been measured near the outer midplane of many fusion devices using three nearby Langmuir probes; and although it is roughly (factor of 2-8) consistent with the total particle loss rate [2–5], some sort of asymmetry is required to fully explain the particle balance [43]. A comparison between the total radial particle flux (inferred from $H_\alpha$ tomography) and turbulent radial fluxes from probes and heavy ion beam probe (HIBP) was made [44] in the TEXT tokamak and is shown in Fig. 2. The good agreement showed for the first time that electrostatic turbulent flux could explain all the radial transport.

Attempts to account for the particle inventory and connect that to global radial fluxes [26,44] were recently done in Alcator C-Mod [36], showing that recycling at the chamber walls was large and increasing with density. As the discharge density was increased, the $n_e$ profile showed increased flattening in the far SOL due to enhanced radial transport. Work at DIII-D [16] determined that intermittent, ballistic, events in the SOL with amplitudes above 2.5× of the rms deviation were responsible for much of the turbulent transport [16,37] and this convective flux can cause large radial transport in regions with a shallow gradient and so

can deposit particles and energy in unexpected places. Intermittent events are seen on many toroidal devices, such as the ADITYA, T-10, CASTOR, DIII-D, MAST and Tore-Supra tokamaks [45–47], and non-tokamaks such as W7-AS, TJ-II, TJ-K, RFX, SINP and HT-7 [48–52]. The intermittency is due to coherent, long-lived filamentary structures that exist within the turbulence and that have been characterized by using imaging [53–55], conditional sampling [16,25,41,45,56] and wavelet analysis [57].

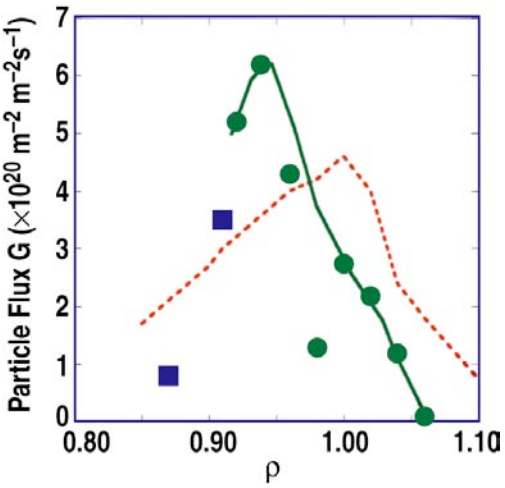


Fig. 2. The particle flux in TEXT [45] deduced from $H_\alpha$ (dashed line), and that measured by probes (circles and solid line) and by HIBP (squares) are superimposed to make the point that turbulent transport can explain the total particle flux.

Fast digital cameras and optical arrays together with image analysis of 2D edge turbulence data have been used to identify 2D turbulence velocity fields in DIII-D [58,59], and also the structure and motion of intermittent coherent structures in Alcator C-Mod, TJ-II, NSTX and W7-AS [41,53,55,60–63]. The BES diagnostic at DIII-D [64] measures ~5 × 6 cm frames every 1 μs and two of them, spaced by 6 μs, are $\delta n/n$ seen in Fig. 3 clearly showing a poloidal cut of filaments and their 2D motion.

Measurements of intermittency in the radial turbulent particle flux extracted from the background using conditional averaging techniques show that the intensity of the flux is much lower in L-mode than in H-mode. Intermittent events lead to positive skewness of signals ($n_e$, $T_e$, $E_\theta$) in the SOL, and negative skewness at or inside the LCFS due to negative events (voids), as seen in DIII-D, and NSTX [16,65] due to interchange instability [66] and also in the linear machine LAPD [67] due to centrifugal forces or neutral wind mechanisms [68]. A density skewness profile obtained from BES at DIII-D in Fig. 4 shows that the void-peak transition occurs at/inside the LCFS.

The radial velocity of intermittent objects, important due to its relationship to transport in the SOL, is of the order of 1 km/s at the LCFS, slows down with increasing radius in the SOL of DIII-D [16], but is roughly constant with minor radius in Alcator C-Mod [41]. The driving mechanism of individual filaments was proposed [67,68] to be the B field curvature creating a local polarization that drives the filaments by $E \times B$ motion. The models have been refined greatly by adding interaction with the neutral background, local ionization and

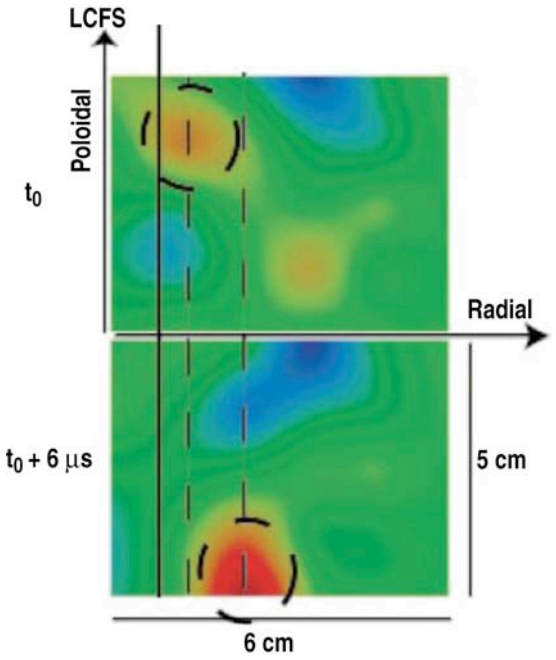


Fig. 3. 2D images of density by BES in DIII-D in the poloidal-radial plane taken 6 $\mu s$ apart showing an intermittent filament moving radially and poloidally.

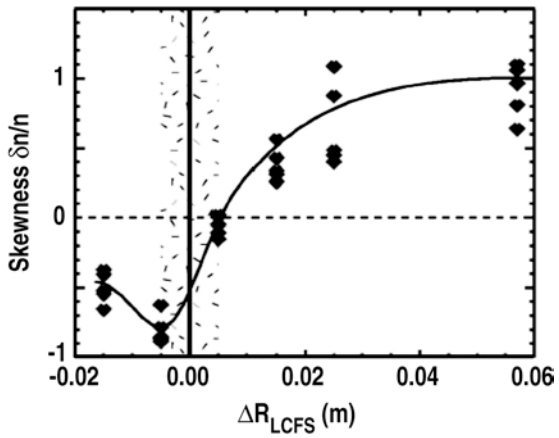


Fig. 4. Skewness profile of BES-measured density fluctuations in DIII-D showing that peaks dominate in the SOL while voids are present inside the LCFS.

better dissipation mechanisms [69–78] and in particular, current loops and circuit paths through the X-point or target plates. In a recent electrostatic two-region model [70], The variation of normalized blob velocity, $\hat{V}$, versus collisionality, $\Lambda$, is predicted, and shown for two normalized blob sizes, $\hat{a}$ ($\hat{a} = 1.3$ "small" and $\hat{a} = 10$ "large"), in Fig. 5:

$$\hat{a} = \frac{a_b}{a_*} = \frac{a_b R^{1/5}}{L_{\|}^{2/5} \rho_s^{4/5}} \quad \hat{V} = \frac{V}{V_*} = \frac{V}{c_s}\left(\frac{R}{a_*}\right)^{1/2} \quad \Lambda = \frac{\nu_{ei} L_{\|}}{\Omega_e \rho_s} \quad . \tag{2}$$

Here $a_b$ and $V$ are the blob size and velocity, $R$ is the major radius, $L_{\|}$ is the connection length, $\rho_s$ is the gyroradius, $\Omega_c$ is the gyro frequency, $\nu_{ei}$ is the collision frequency, and $C_s$ is the sound speed. Notice that at low $\Lambda$, large blobs are 20x faster than small blobs but at

large $\Lambda$ all sizes move fast. Two analytical curves representing the functional dependence are compared to "measurements" from a turbulence simulation (dots) [70] and have been successfully compared to experimental data [75], indicating that fair understanding of the individual filament transport in various regimes has been achieved.

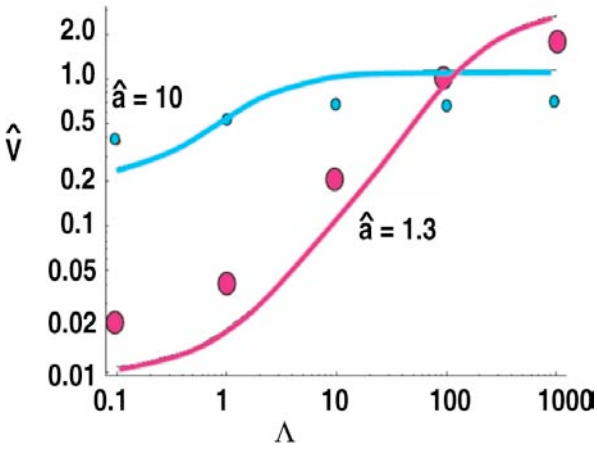


Fig. 5. Intermittent filament normalized velocity versus normalized collisionality for two initial filament poloidal sizes of $\hat{a}$ = 1.3 and 10, the lines denote analytical calculations and the dots simulation results.

Evidence shows that the turbulent transport and fluctuation intensity is not uniform in the poloidal cross-section. In-out asymmetries were observed in the CCT and CASTOR [78,79] tokamaks, and a significantly lower relative density fluctuation level, turbulence size and turbulent radial transport were seen on the high field side SOL of the T-10 tokamak [80,81]. In Alcator C-Mod [62,82], the relative $J_{sat}$ fluctuation level in the HFS SOL was up to 10 times lower than that on the same flux surface at the LFS SOL. The source of radial transport asymmetries is understood as magnetic curvature and X-point shear [83], and they should be tallied in both the particle and energy inventories feeding the SOL.

A definitive scaling of edge turbulence has not yet been achieved [84] although attempts have been made to perform scaling with local and global parameters on many devices such as the Caltech, TEXT, Alcator C-Mod and DIII-D tokamaks [36,37,85,86] and in the W7-AS stellarator, where little dependence was observed [1–6,85,87–89]. Recent studies in ASDEX, TEXTOR, DIII-D Alcator C-Mod, TCV and MAST [36,45,75,77,87,90] seem to reveal a reproducible dependence with collisionality involving ***local*** $T_e$, $N_e$ and also $L_{||}$. Systematic scans in TEXT [85] did not show a variation of $\delta n/n$ with $\rho_s/L_n$ and recent results considering intermittency seem to contradict it. Data from DIII-D obtained during a density scan (from 2.7 to $5.2\times10^{13}$ cm$^{-3}$) showed a clear increase of the intermittent filament's density and radial flux. Newer results need to be married to older ones where the relative edge density fluctuation level was roughly independent of $I_p$ and edge safety factor $q$(a) (i.e. $L_{||}$) in the ASDEX and TEXT tokamaks [85,87] and with the similarity between edge turbulence of tokamaks and stellarators.

## 2.2. TRANSPORT BARRIERS

The edge plasma sets the boundary conditions for many processes in the core, and in turn these processes cause a change in edge parameters, thus the dynamics in the edge are quite complex [91,92]. A velocity shear layer was identified [28] in the boundary of tokamaks and stellarators by measuring the phase velocity of the turbulence in the poloidal direction [28,93], which changes sign from the electron diamagnetic drift direction inside the last closed flux surface to the ion diamagnetic drift direction in the SOL [94]. The shear layer is correlated with the reduction of turbulence [95], effect that has been verified in many devices [45,96–99] and can be responsible for the formation of an edge transport barrier resulting on a spontaneous transition from low (L-mode) to high (H-mode) [100] confinement, a bifurcation process. However, the process was only fully verified when H-mode-like behavior was obtained after a velocity sheared region was introduced artificially via an externally applied radial electric field [101,102]. Data from an electrode-biased discharge in TEXTOR is displayed in Fig. 6, where it is shown that as the radial electric field is increased gradually, the turbulent radial flux decreases across the LCFS, creating a transport barrier.

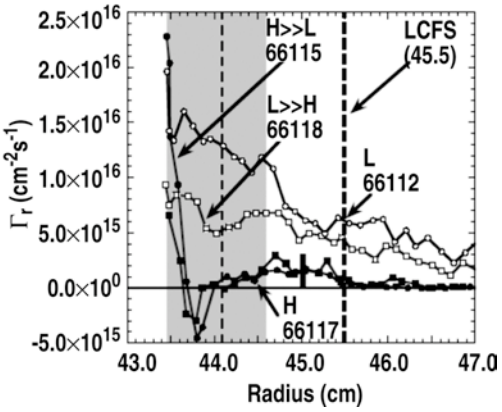


Fig. 6. Radial profiles of turbulent radial particle flux for various applied electrode voltages (0, 100, 400 and 100 V) in TEXTOR. As the field grows in the shaded region, and the $E \times B$ shear increases, the radial particle flux is reduced. The plasma conditions are labeled as H-mode like, L-mode like and transitional (L-H or H-L).

Measurements showed a sudden decrease in fluctuations of edge potential and density at the L–H transition [103] where density turbulence levels usually drop but often recover to their L-mode levels later in the H-mode phase [37,104–108]. A reduction in $T_e$ fluctuations was associated with the shear flow in biased H-modes in TEXTOR [29] and changes have been seen in the phase and correlation coefficient between the density and potential fluctuations, leading to a reduction in the turbulent transport rate [99,109]. Finally, changes were seen at the L–H transition in DIII-D in the intermittency [45], bi-spectral coupling [110] and nonlinear dynamics [111], indicating they are all interconnected.

The mechanism of shear stabilization of turbulence and $E \times B$ drifts has been used repeatedly to manipulate the edge plasma and achieve H-mode-like conditions [112]. Early work was conducted in TEXTOR, TdV and DIII-D [113–115] using limiter and divertor bias with the main result that the SOL thickness was manipulated but little changed in core performance. In CCT, TEXTOR and KT-5C [101,116,117], an electrode was inserted in the

core, generating H-mode-like core conditions; however, this method is not suitable to high power discharges. Experiments applying ergodic layers in Tore-Supra, TEXTOR and DIII-D and W7-AS [118–120] have produced significant changes in particle transport/balance as well as turbulence modification.

The origin of the naturally occurring shear flows has been credited to the Reynolds stress $R$ ($R = -\delta v_{rad}\delta v_{pol}$), which causes the rate of momentum transfer between the mean flow and the turbulence [54], and there is active research in the TJ-II stellarator, the ISTTOK, HT-6M and HT-7 tokamaks [121–124] and the H-1 heliac [125], with some measurements verifying the Reynolds stress thesis and others not fully in agreement with it [126].

## 2.3. HEAT TRANSPORT

Heat transport is a crucial element for next generation devices because the heat flux to the target plates is close to the engineering limits and strong parallel heat transport is dominant. Although the heat deposition during Type I ELMs is the main concern, inter-ELM heat transport must be also understood. The radial ***electron*** (i.e. not ions) heat transport can be due to electrostatic and magnetic fluctuations, although the latter has been measured to be negligible [127,128]. We can write [$\Gamma_r^{ES}$ is given by Eq. (1)] the electrostatic radial heat flux:

$$Q_r^{ES} = \langle nT_e\tilde{v}_r\rangle \approx \frac{3}{2}kT_e\Gamma_r^{ES} + \frac{3}{2}\frac{n_e}{B_\varphi}\langle k\tilde{T}_e\tilde{E}_\theta\rangle = Q_{conv} + Q_{cond} \quad , \tag{3}$$

Recent DIII-D measurements of electrostatic conductive and convective radial heat flux profiles at the midplane are shown in Fig. 7 for L- and H-mode discharges. In L-mode, the convective heat flux [Fig. 7(a)] is larger than the conductive flux [Fig. 7(b)] in the near SOL and of the same order in the far SOL. In H-mode, both components are of similar magnitude across the SOL. A comparison between L- and H-mode total heat flux profiles [Fig. 7(c)] indicates that the H-mode flux is much larger than the L-mode flux but only over a very narrow (0.5 cm) range. These measurements account for the ***full*** power balance if the flux existed over a uniform band at the outer midplane only 1 m wide poloidally. The heat conduction, $Q_{cond}$, term was measured to be significant in TEXTOR [116] and measurements in TEXT comparing power balance analysis to the electrostatic heat transport found that 80% could be accounted by electrostatic convection and 20% by conduction [129].

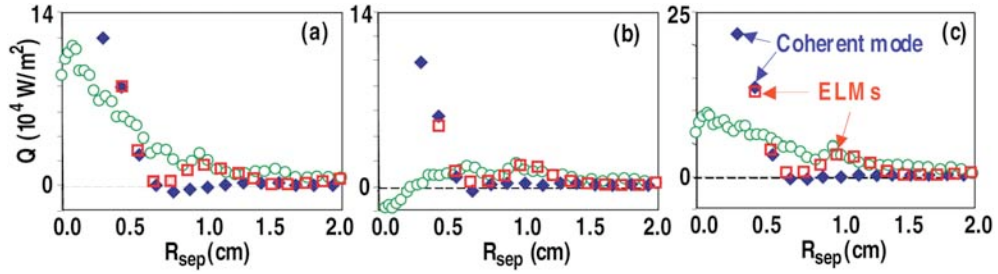


Fig. 7. Radial profiles of (a) convective heat flux, (b) conducted heat flux, and (c) total heat flux in L-Mode (circles) and H-mode (diamonds and squares) DIII-D discharges. Some ELMs are indicated.

# 3. ELMS

A source of energy and particles into the edge/SOL is the plasma transported by ELMs, and is considered a critical issue for the viability of ITER since it could deposit up to 3%–8% of the discharge energy onto the walls [130], well above engineering limits. Furthermore, experiments have shown that ELM pulses can reach the main chamber walls and thus become a threat to regions not previously believed to need protection. We discuss Type I ELMs. Much of the known dynamics and theoretical understanding of ELMs has been recently reviewed [131], highlighting JET measurements. Edge/SOL measurements of plasma flux, $T_e$, $n_e$ [132] and hot ion flux, are consistent with part of the ELM energy loss being in the form of a series of field aligned filaments expelled at discrete toroidal locations in the outboard midplane [133]. Evidence is verified by fast visible [134] and IR camera systems in ASDEX-U and JET [134], which observed helical stripes of power deposition during ELMs on main chamber and divertor targets. Findings are that $T_e$ in the ELM filament reaching the wall remains low but the plasma densities at the wall are collisionality (i.e. ELM size) and pedestal density dependent with the result that the electron-convected energy can also be sizable and thus heat loads at the wall can be significant. In DIII-D, SOL profile measurements of $n_e$, $T_e$, and $n_e$ fluctuations during L-mode and ELMing (Type I) plasma H-mode indicate that: (1) the peak ELM density decays quickly but still maintains about 1/4 of the original LCFS density, (2) $T_e$ decays much faster, with roughly 1/10 of the LCFS temperature left at the wall and (3) plasma parameters during ELMs often surpass in values those during L-mode.

A key finding [2,3] is that ions arrive at the SOL with energies characteristic of the pedestal region, as expected on the basis of a new transient model of ELM filament energy loss [3,4] which reproduces the observed trend seen in JET for larger ELMs to deposit less energy in the divertor. Among the unexplained features are the observed target plate load asymmetry and the heat deposited in the mid-far SOL, which does not seem to obey either electron conduction or sheath-limited regimes. An interesting issue is that ELM-mediated transport is traditionally assumed to overcome inter-ELM turbulent transport. However, it has been recently demonstrated [4], and can be seen in Fig. 8 that the fraction of ion flux due to ELMs is ~100% at low collisionality, but is reduced to ~30% at high collisionality, since ELMs become smaller as intermittent transport increases.

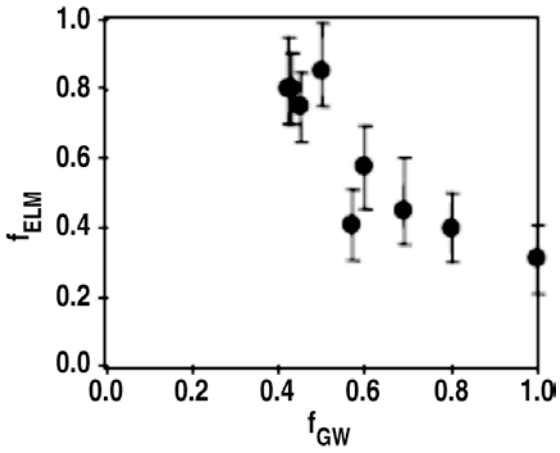


Fig. 8. The fraction of ion flux at DIII-D's wall due to ELMs compared to the total ion flux ( $f_{\mathrm{ELM}}$ ) versus discharge density/collisionality (expressed in Greenwald fraction, $f_{\mathrm{GW}}$ ).

# 4. SOL FLOWS

Once particles and heat are exhausted from the core due to radial transport across the LCFS, parallel transport becomes a crucial player. Particle transport along the magnetic field lines in the SOL is crucial for particle (including impurity) control, energy transport, and impurity generation, and has important implications on the choice and design of plasma facing components [130]. The classical view of flow along the field lines consists of low pressure points at the divertor plates with an stagnation point quasi-symmetrically located near the plasma crown and plasma flowing towards the target plates both in the low field side (LFS) and high field side (HFS). Significant progress has been made in understanding the driving mechanisms in SOL mass transport along the magnetic field lines by using Mach probes at various poloidal locations in multiple devices, together with interpretative modeling. All results showed common SOL flow patterns recognizing new factors such as LFS-enhanced asymmetry in diffusion and classical drifts in addition to the classical view of pressure differences along the flux tube controlling the flow velocity.

## 4.1. OBSERVATIONS

We will review recent measurements, mainly SOL flow in L-mode diverted tokamak plasmas, that have been performed in various tokamaks. Figure 9 summarizes measurements from JT-60U, JET, Alcator C-Mod, TCV, DIII-D, ASDEX-Upgrade (AUG) and Tore Supra [82,135–142]. In single-null divertor configuration with the ion $B \times \nabla B$ drift direction towards the divertor, and medium plasma density, $n_e/n_{GW} \sim 0.4$–$0.45$, the Mach profiles in the near-mid SOL indicate that the stagnation point is near and below the outer midplane. Measurements in the HFS SOL (JT-60U, C-Mod) show that $M_{||}$ reaches near sonic levels (0.5–1), whereas measurements of $M_{||}$ in the narrow region near the separatrix show no (C-Mod) or small flow towards the plasma top ( $M_{||} \sim 0.15$ in JT-60U). In the LFS, SOL flow towards the divertor was observed in JT-60U [135], DIII-D [140] and AUG with typical $M_{||}$ near the separatrix of 0.4–0.5, as seen in Fig. 9, suggesting that the stagnation point is between the LFS midplane and the X-point. In short, the plasma is flowing away from slightly below the midplane, upwards toward the HFS divertor and downwards towards the LFS divertor, reaching a maximum in the HFS.

From the existing multi-machine data, the following observations can be made, namely that the direction of flow can be reversed when $B_T$ is reversed and that there is a trend towards a lower, single, offset value of $M_{||}$ in the near SOL with increasing $n_e$ (LFS midplane in C-Mod and at the plasma top in JET). At the LFS midplane (C-Mod, JT-60U and TCV) the direction of the SOL flow changes with $B_T$ reversal as seen in Fig. 9. In the plasma crown at DIII-D (Fig. 10), $M_{||}$ is small and toward the LFS when $\nabla B$ is away from the X-point and large when $\nabla B$ is toward the X-point, flowing toward the HFS.

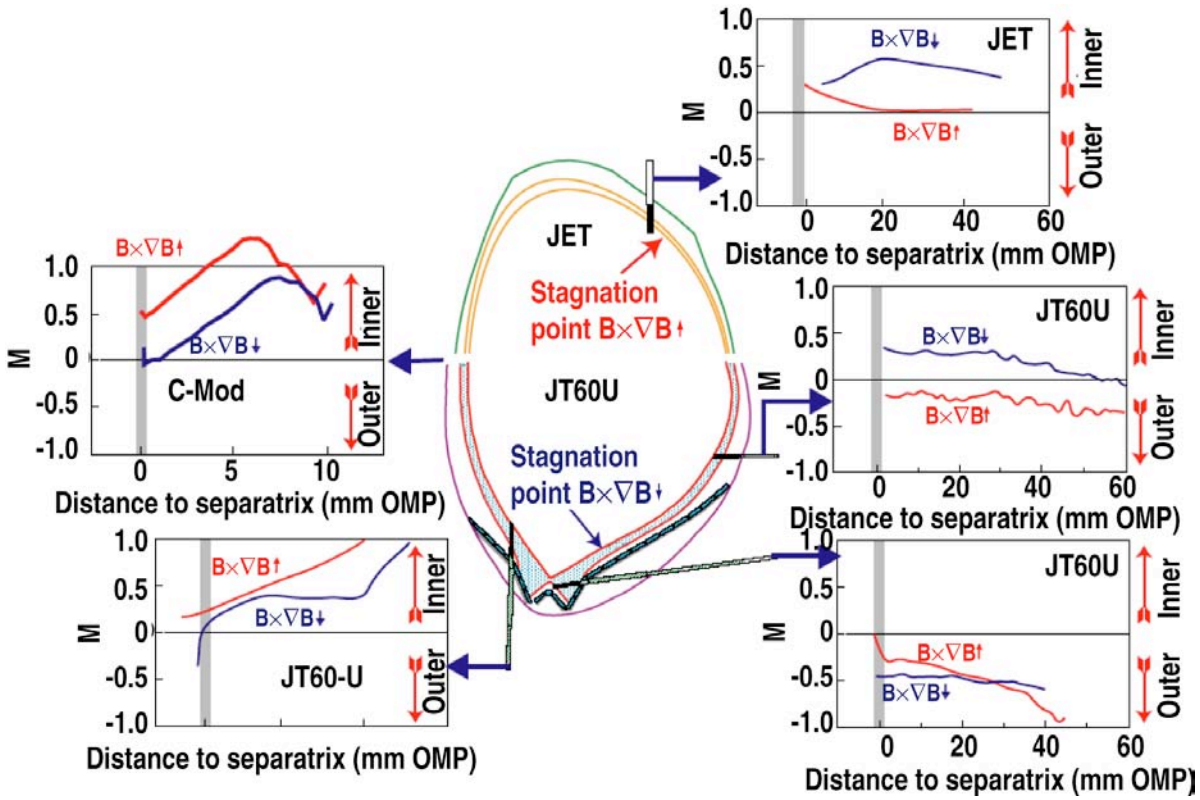


Fig. 9. Measurements of the Mach number on various poloidal locations in JT-60U and JET for $\nabla B$ towards/away from the X-point.

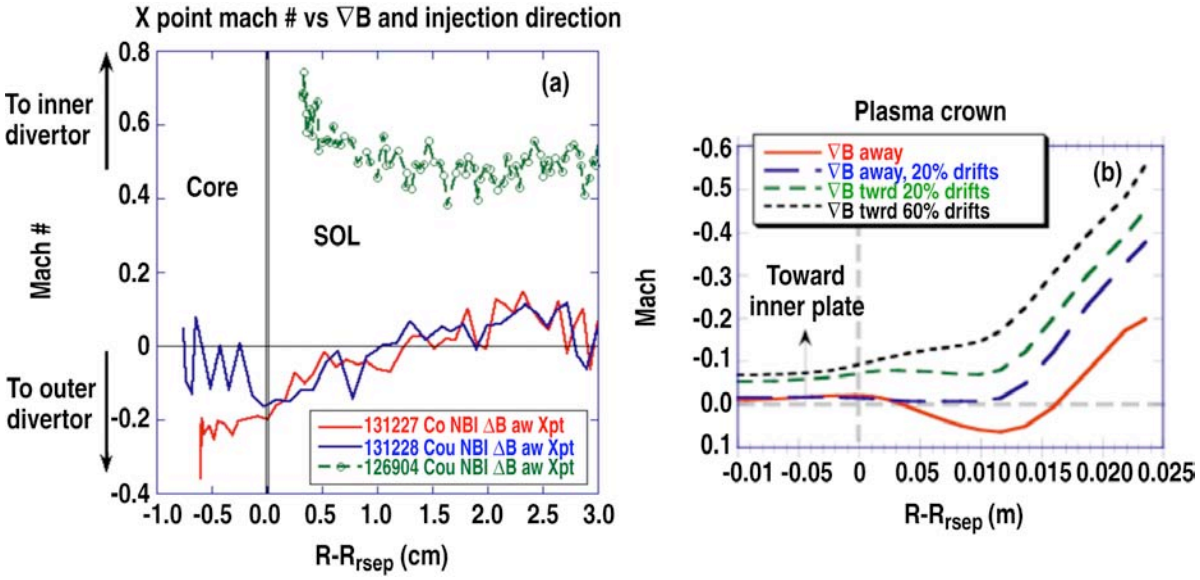


Fig. 10. (a) Radial profiles of measured Mach number at the plasma crown in L-mode discharges at DIII-D for $\nabla B$ away from the X-point (solid lines, co and counter injection) and $\nabla B$ towards the X-point (dashed line). (b) UEDGE simulations of the $M_{\parallel}$ at the same location and $\nabla B$ direction cases while varying the strength of the classical drifts.

In various devices (Alcator C-Mod, JT-60U and TCV) an offset, circa $M_{||} \sim 0.3$, appears by changing $n_e$ at fixed $B_T$, which suggests that a $B_T$-independent component of the SOL flow is produced towards the HFS SOL, and that it is comparable to the $B_T$-dependent component. In short, there is a $B_T$ direction-dependent component (classical drifts and edge rotation) and $B_T$-independent component (in-out asymmetry in edge diffusion and divertor detachment) combining into complicated SOL flow pattern.

## 4.2. FLOW-INDUCING MECHANISMS

A variety of classical drifts ($E \times B$ and $B \times \nabla B$) play a role in transport in toroidal geometry [142] and recently, the role of ion Pfirsch-Schlüter's flow, due to in-out asymmetry of $E_r \times B$ and $\nabla B$ drifts, has been elucidated [143–145]. The P-S flow has the flow direction against the ion $B \times \nabla B$ drift, and the analytical expression [145] in confined plasma, $V_{||}^{PS} = 2q\left(E_r - \nabla p_i / e n_i\right)\cos\theta / B$ ($q$ is the safety factor, $\theta$ is the poloidal angle) has a maximum at the midplane. Evaluation of $V^{PS}$ was done at the LFS midplane for normal and reversed $B_T$ cases in JT-60U [146] and in TCV [139] where the calculated value of $V^{PS}$ (normalized by the sound speed), shown in Fig. 11, matches the measured values of $M_{||}$ for a variety of conditions. On the other hand, effects of changing $B_T$ appear to be large on the top of the plasma in various devices (JET, DIII-D and JT60-U) in a region where the PS drift effect is supposed to be small, so other mechanisms are required.

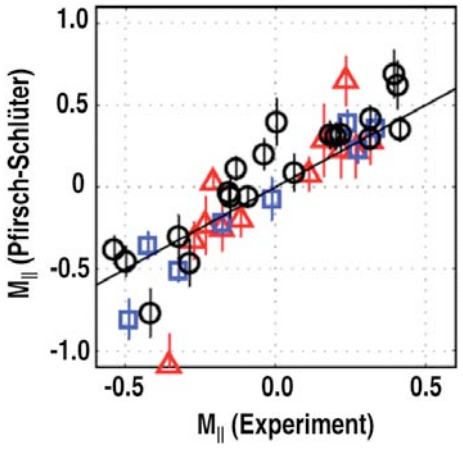


Fig. 11. Comparison of the calculated $M_{||}$ due to PS mechanism versus the experimental measurements of $M_{||}$ at the midplane of TCV for various plasma conditions showing remarkable agreement.

To clarify the role and strength of a drift-independent mechanism driving parallel flows, hypothesized to be a pressure peak at the midplane caused by the ballooning character of the turbulent transport, experiments were performed in Alcator C-Mod and TCV [82,139]. SOL plasma flow profiles were examined while the geometry was changed (LSN, USN and DN for Alcator only) and, at TCV [139], the profiles taken above and below the effective midplane for the USN and LSN were subtracted to eliminate the contribution of the drift terms, revealing an offset, drift-free component [139] which disappeared at the midplane. In Alcator, the measurements of flow along the field line and pressure at two points (HFS, LFS)

were compared [82] concluding that the plasma flow was enhanced by higher static pressure in the HFS, considered to be caused by the larger radial turbulent flux ballooning.

Experiments at DIII-D [140,147] showed the parallel Mach number in the divertor region, which increases monotonically from $M_{||} \sim 0.2$ near the X-point to $M_{||} \sim 1.0$ at the target plate, suddenly increased to $M_{||} = 1.0$ (i.e. sonic flow) across the whole divertor upon detachment. The plasma velocity did not change ($T_e$ dropped), however the mass and momentum flow increased by factors of 3 due to the density augmentation. In JT-60U [136], the HFS $M_{||}$ profile shows increased flow towards the HFS divertor during detachment and such increase is more marked in the far SOL (2x) than in the near SOL. Recent DIII-D experiments [148] show that divertor pumping can cause a 100% change in the near SOL $M_{||}$ midplane profile, as shown in Fig. 12. Therefore, the classical view that the target plate conditions are important drivers for parallel flows is still quite relevant.

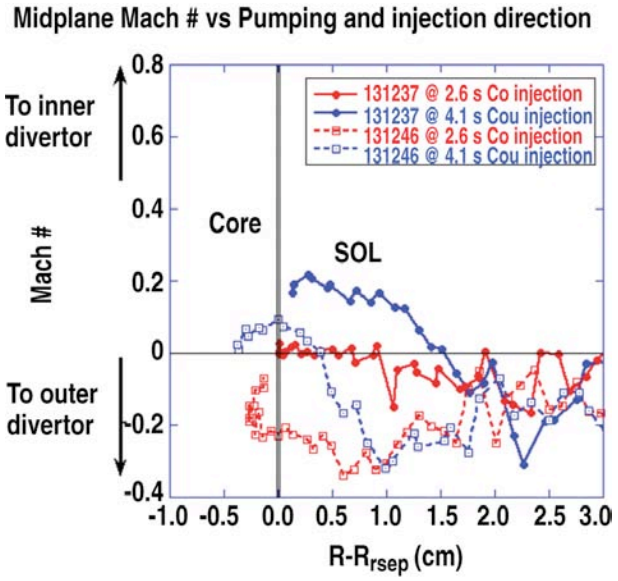


Fig. 12. Profiles of Mach number at the midplane in L-mode discharges in DIII-D for co- (red) and counter-injection (blue) cases with (dashed lines) and without (solid lines) divertor pumping. Flow is shifted to the outer divertor by pumping.

The SOL and core plasma can also exchange momentum due to diffusion, convection and viscosity, contributing to other sources of flow. The relationship between the edge rotation and SOL flow was investigated in C-Mod [149] in plasmas without external momentum input concluding that SOL flows affect the core rotation via an as yet unidentified mechanism. Conversely, recent DIII-D experiments [148] in L-mode with NBI heating varied from co to counter injection (relative to $I_p$), have shown that the edge/SOL flow can follow the core flow indicating *outward* momentum transport across the LCFS. Mach profiles shown in Fig. 12 for pumped (dashed lines) and unpumped, otherwise identical discharges show a significant difference if the core is co- or counter-injected. Investigation of the coupling between the edge and SOL plasmas is important to understand not only the SOL flow but also edge rotation physics in the plasma boundary.

## 4.3. MODELING AND UNDERSTANDING

The state of turbulent transport theory has been recently reviewed [150]. Drift effects have been implemented into 2D edge transport codes with realistic magnetic geometries such as UEDGE [151,152], EDGE2D/Nimbus [137,153,154] and B2SOLPS5.0 [155,156], and simulations lead to SOL flow patterns in qualitative agreement with those observed experimentally. Results from UEDGE simulations of flows in DIII-D can be seen in Fig. 10(b) showing that although the effect of drifts is properly reflected in the simulated flow, the magnitude is underestimated by a factor of 2–3. EDGE2D simulations of JET L-mode plasmas for the normal and reversed $B_T$ [153] reproduce a shift of the stagnation point and the observed direction of the flow but not the magnitude of the flow by factors of 2–3. Simulations have difficulty in generating fast SOL flows in the far SOL which is crucial for neutral and impurity recycling at the first wall [152]. The B2SOLPS5.0 simulation for C-Mod [156] achieved the experimentally observed values at the LFS midplane but the simulation is very sensitive to the calculation of the electric fields across the LCFS and SOL. A variety of improvements are implemented in the existing fluid codes, such as enhanced diffusion at the LFS edge (such as $D_\perp \sim 1/B$) [157–159], different momentum coupling physics across the LCFS, torque generation due to difference in surface averaged $j_r$ [160], and anomalous momentum transfer (Reynolds stress) [161] for different tokamak geometries in order to understand the effects on the SOL flow. However, there is a growing awareness [162] that kinetic modeling may be necessary to properly reproduce the measurements and that will be a significant numerical challenge.

# 5. SUMMARY

Significant progress has been made in the last few years in the understanding of radial anomalous particle transport and asymmetries and analytical and numerical tools have been developed. Intermittent transport has been characterized and good understanding has emerged of its source, dynamics across the SOL and some scaling parameters. Work on ELMS characterization, in particular fast imaging, fast SOL measurements and the development of numerical tools exploring the peeling-ballooning physics explore the principles ruling ELM birth and dynamics in the SOL. These topics have been the focus of attention due to the ELM's potential to breach engineering limits in ITER. Understanding of parallel flows in the SOL has benefited from verification and integration of old mechanisms, ballooning of radial transport and the newly found P-S drive into a more global paradigm that has been incorporated into fluid codes. Work on thermal transport characterization and understanding is commencing and it presents significant challenges due to the need for fast $T_e$ and $T_i$ diagnostics. Finally, new work suggests there are EM effects at play in the pedestal [163].

# REFERENCES

[1] C.M. Surko et al., Science 221 (1983) 817.
[2] P.C. Liewer, Nucl. Fusion 25 (1985) 1281.
[3] A.J. Wootton et al., Phys. Fluids B 2 (1990) 2879.
[4] B.A. Carreras, IEEE Trans. Plasma Sci. 25 (1997) 1281.
[5] M. Endler, J. Nucl. Mater. 266–269 (1999) 84.
[6] W. Horton, Rev. Mod. Phys. 71 (1999) 735.
[7] C. Hidalgo, Plasma Phys. Control. Fusion 37 (1995) A53.
[8] B.A. Carreras, J. Nucl. Mater. 337–339 (2005) 315.
[9] E. Powers, Nucl. Fusion 14 (1974) 749.
[10] J.M. Beall et al., J. Appl. Phys. 53 (1982) 3933.
[11] E. Sánchez et al., Plasma Phys. 7 (2000) 1408.
[12] B.P. van Milligen et al., Phys. Plasmas 2 (1995) 3017.
[13] J.S. Kim et al., Phys. Rev. Lett. 79 (1997) 841.
[14] G.R. Tynan et al., Phys. Plasmas 8 (2001) 2691.
[15] A.E. White et al., Phys. Plasmas 13 (2006) 072301.
[16] J.A. Boedo et al., Phys. Plasmas 8 (2001) 4826.
[17] V. Budaev et al., Nucl. Fusion 44 (2004) S108.
[18] B. Carreras et al., Phys. Plasmas 5 (1998) 3632.
[19] R. Jha et al., Phys. Plasmas 10 (2003) 699.
[20] B.D. Dudson et al., Plasma. Phys. Control. Fusion 47 (2005) 885.
[21] B.A. Carreras et al., Phys. Plasmas 6 (1999) 1885.
[22] E. Spada et al., Phys. Rev. Lett. 86 (2001) 3032.
[23] R. Sanchez et al., Phys. Rev. Lett. 90 (2003) 185005.
[24] S.J. Levinson et al., Nucl. Fusion 24 (1984) 527.
[25] D.L. Rudakov et al., Plasma Phys. Control. Fusion 44 (2002) 717.
[26] R.A. Moyer et al., J. Nucl. Mater. 241–243 (1997) 633.
[27] R.D. Durst et al., Phys. Rev. Lett. 71 (1993) 3135.
[28] C.P. Ritz et al., Phys. Rev. Lett. 62 (1989) 1844.
[29] J.A. Boedo et al., Phys. Rev. Lett. 84 (2000) 2630.

[30] M.A. Meier et al., Phys. Rev. Lett. 87 (2001) 085003.
[31] R. Kumar et al., Nucl. Fusion 43 (2003) 622.
[32] V. Pericoli-Ridolfini et al., Nucl. Fusion 38 (1998) 1745.
[33] C. Silva et al., Rev. Sci. Instrum. 75 (2004) 4314.
[34] S.J. Zweben et al., Nucl. Fusion 21 (1981) 193.
[35] J. Stockel et al., Plasma Phys. Control. Fusion 41 (1999) A577.
[36] B. LaBombard et al., Phys. Plasmas 8 (2001) 2107.
[37] D.L. Rudakov et al., Nucl. Fusion 45 (2005) 1589.
[38] D.L. Winslow et al., Rev. Sci. Instrum. 68 (1997) 396.
[39] H. Thomsen et al., Phys. Plasmas 9 (2002) 1233.
[40] D.H.J. Goodall, J. Nucl. Mater. 111–112 (1982) 11.
[41] O. Grulke et al., Phys. Plasmas 13 (2006) 012306.
[42] S.J. Zweben et al., Phys. Fluids B 1 (1989) 2058.
[43] G.R. Tynan et al., Phys. Rev. Lett. 68 (1999) 3032.
[44] A.J. Wooton et al., Plasma Phys. Control. Fusion 30(11) (1988) 1479.
[45] J.A. Boedo et al., Phys. Plasmas 10 (2003) 1670.
[46] R. Jha et al., Phys. Rev. Lett. 69 (1992) 1375.
[47] G.S. Kirnev et al., J. Nucl. Mater. 337 (2005) 352.
[48] V. Carbone et al., Phys. Plasmas 7 (2000) 445.
[49] B.Ph. van Milligen et al., Phys. Plasmas 12 (2005) 052507.
[50] F. Sattin et al., Phys. Plasma 11 (2004) 5032.
[51] S.K. Saha et al., Phys. Plasmas 13 (2006) 092512.
[52] G.S. Xu et al., Phys. Plasmas 13 (2006) 102509.
[53] S.J. Zweben et al., Nucl. Fusion 44 (2004) 134.
[54] J.A. Alonso et al., Plasma Phys. Control. Fusion 48 (2006) B465.
[55] S.J. Zweben, Phys. Fluids 28 (1985) 974.
[56] O. Grulke et al., Plasma Phys. Control. Fusion 43 (2001) 525.
[57] L. Dong et al., Phys. Rev. E 57 (1998) 5929.
[58] G.R. McKee et al., Phys. Plasmas 10 (2003) 1712.
[59] C. Holland et al., Rev. Sci. Instrum. 75 (2004) 4278.
[60] J.L. Terry et al., J. Nucl. Mater. 337–339 (2005) 322.
[61] T. Munsat, Rev. Sci. Instrum. 77 (2006) 103501.

[62] G.R. McKee et al., Rev. Sci. Instrum. 75 (2004) 3490.

[63] J.L. Terry et al., Phys. Plasmas 10 (2003) 1739.

[64] S.J. Zweben et al., Phys. Plasmas 13 (2006) 056114.

[65] J.A. Boedo et al., Nucl. Fusion submitted (2008).

[66] Y. Sarazin, Ph. Ghendrih, Phys. Plasmas 5(12) (1998) 4214-28; P. Beyer et al., Plasma Phys. Control. Fusion 41, Suppl. 3A (1999) A757-69; Y. Sarazin et al., Phys. Plasmas 7(4) (2000) 1085-8.

[67] T.A. Carter, Phys. Plasmas 13 (2006) 010701.

[68] S.I. Krasheninnikov, D.A. D'Ippolito, and J.R. Myra, Phys. Plasmas 74 (2008) 679.

[69] S.I. Krasheninnikov, Phys. Lett. A 283 (2001) 368.

[70] J.R. Myra, D.A. Russell, D.A. D'Ippolito, Phys. Plasmas 13 (2006) 112502; D.A. Russell, J.R. Myra, and D.A. D'Ippolito, Phys. Plasmas 14 (2007) 102307.

[71] A.Yu. Pigarov et al., J. Nucl. Mater. 313–316 (2003) 1076.

[72] S.I. Krasheninnikov, D.D. Ryutov, G.Q. Yu, J. Plasma Fusion Res. 6 (2005) 139.

[73] D.A. Russell, D.A. D'Ippolito, J.R. Myra, W.M. Nevins, X.Q. Xu, Phys. Rev. Lett. 93 (2004) 265001.

[74] G.Q. Yu and S.I. Krasheninnikov Phys. Plasmas 10(11) (2003) 4413-4418.

[75] J.R. Myra et al., Phys. Plasmas 13 (2004) 4267.

[76] O.E. Garcia, V. Naulin, A.H. Nielsen, J. Juul Rasmussen, Phys. Rev. Lett. 92 (2004) 165003.

[77] O.E. Garcia, N.H. Bian, J.-V. Paulsen, S. Benkadda, K. Rypdal, Plasma Phys. Control. Fusion **45** (2003) 919.

[78] J.R. Myra and D.A. D'Ippolito, Phys. Plasmas 12 (2005) 092511.

[79] G. Tynan et al., Plasma Phys. Control. Fusion 38 (1996) 1301.

[80] V.A. Vershkov et al., J. Nucl. Mater. 241–243 (1997) 873.

[81] G.S. Kirnev et al., Nucl. Fusion 45 (2005) 459.

[82] B. LaBombard et al., Nucl. Fusion 44 (2004) 1047.

[83] M. Endler, Plasma Phys. Control. Fusion 41 (1999) 1431.

[84] M.A. Pedrosa et al., Phys. Plasmas 2 (1995) 2618.

[85] G.R. McKee et al., Nucl. Fusion 41 (2001) 1235.

[86] M. Ramisch et al., Phys. Plasmas 12 (2005) 032504.

[87] T.L. Rhodes et al., Nucl. Fusion 33 (1993) 1147.

[88] G.D. Conway et al., Plasma Phys. Control. Fusion 47 (2005) 1165.

[89] J.L. Terry et al., Nucl. Fusion 45 (2005) 1312.

[90] M. Endler et al., Nucl. Fusion 35 (1995) 1307.

[91] C.P. Ritz et al., Phys. Fluids 27 (1984) 2956.

[92] V. Antoni et al., Plasma Phys. Control. Fusion 47 (2005) B13.

[93] C. Hidalgo et al., Plasma Phys. Control. Fusion 43 (2001) A313.

[94] C.P. Ritz et al., Phys. Rev. Lett 65 (1990) 2543.

[95] H. Biglari, P.H. Diamond, P.W. Terry, Phys. Fluids B 2(1) (1990) 1.

[96] M.A. Pedrosa et al., Plasma Phys. Control. Fusion 47 (2005) 777.

[97] G.R. Tynan, L. Schmitz, R.W. Conn, R. Doerner, R. Lehmer, Phys. Rev. Lett. 68(20) (1992) 3032-5.

[98] G.R. Tynan et al., Plasma Phys. Control. Fusion 36(7A) (1997) A285-90.

[99] R.A. Moyer et al., Phys. Plasmas 2(6) (1995) 2397.

[100] F. Wagner et al., Phys. Rev. Lett. 49(19) (1982) 1408.

[101] R.J. Taylor, P. Pribyl, G.R. Tynan, B.C. Wells, Plasma Phys. Control. Fusion 36(7) (1994) A105.

[102] R.R. Weynants et al., Plasma Phys. Control. Fusion, Vol. II (1993) 251.

[103] K. Ida et al., Fusion Sci. Technol. 49 (2006) 122.

[104] G. Wang et al., Plasma Phys. Control. Fusion 46 (2004) A363.

[105] T. Ido et al., Phys. Rev. Lett. 88 (2002) 055006.

[106] R.A. Moyer, Plasma Phys. Control. Fusion 41 (1999) 243.

[107] R.A. Moyer et al., J. Nucl. Mater. 266 (1999) 1145.

[108] W. Schoppa and F. Hussain, J. Fluid Mech. 453 (2002) 57.

[109] G. Tynan et al., Plasma Phys. Control. Fusion 36 (1994) A285.

[110] R.A. Moyer et al., Phys. Rev. Lett. 87 (2001) 135001.

[111] R.A. Moyer et al., Plasma Phys. Control. Fusion 38 (1996) 1273.

[112] G. Van Oost et al., Plasma Phys. Control. Fusion 45 (2003) 621.

[113] M.J. Schaffer et al., Nucl. Fusion 32(5) (1992) 855.

[114] D. Lafrance et al., Phys. Plasmas 4(10) (1997) 3644.

[115] R.P. Doerner et al., Nucl. Fusion 34(7) (1994) 975.

[116] J.A. Boedo et al., Nucl. Fusion 40 (2000) 1397.

[117] C. Wang et al., IEEE Trans. Plasma Sci. 30 (2002) 625.

[118] P. Devynck et al., Nucl. Fusion 42 (2002) 697.

[119] Y. Xu et al., Phys. Rev. Lett. 97 (2006) 165003.

[120] H. Thomsen et al., Plasma Phys. Control. Fusion 47 (2005) 1401.
[121] C. Hidalgo et al., Plasma Phys. Control. Fusion 42 (2000) A153.
[122] C. Hidalgo et al., Phys. Rev. Lett. 83 (1999) 2003.
[123] Y.H. Xu et al., Phys. Rev. Lett. 84 (2000) 3867.
[124] G.S. Xu et al., Phys. Rev. Lett. 91 (2003) 125001.
[125] H. Xia et al., Phys. Plasmas 11 (2004) 561.
[126] E. Sanchez et al., J. Nucl. Mater. 337 (2005) 296.
[127] G. Fiksel et al., Phys. Rev. Lett. 72 (1994) 1028.
[128] G. Fiksel, Phys. Rev. Lett. 75 (1995) 3866.
[129] C. Silva et al., Plasma Phys. Control. Fusion 48 (2006) 727.
[130] A. Loarte et al., Phys. Plasmas 11 (2004) 2668.
[131] R.A. Pitts et al., Nucl. Fusion 47 (2007) 1437.
[132] J.A. Boedo, D.L. Rudakov, E. Hollmann, Phys. Plasmas 12(7) (2005) 725.
[133] J.A. Boedo et al., J. Nucl. Mater. 337–339 (2005) 771-5.
[134] G.F. Matthews, J. Nucl. Mater. 337–339 (2005) 1.
[135] N. Asakura et al., Nucl. Fusion 39 (1999) 1983.
[136] N. Asakura et al., Plasma Phys. Control. Fusion 44 (2002) 2101.
[137] S.K. Erents et al., Plasma Phys. Control. Fusion 46 (2004) 1757.
[138] B. LaBombard et al., J. Nucl. Mater. 241–243 (1997) 149.
[139] R.A. Pitts et al., J. Nucl. Mater. 363–365 (2007) 505.
[140] J.A. Boedo et al., J. Nucl. Mater. 266–269 (1999) 783.
[141] H.W. Muller et al., J. Nucl. Mater. (2006).
[142] J.P. Gunn et al., J. Nucl. Mater. (2007).
[143] W. Fundamenski et al., J. Nucl. Mater. 337–339 (2005) 305.
[144] P.C. Stangeby, A.V. Chankin, Nucl. Fusion 36 (1996) 839.
[145] A.V. Chankin et al., Nucl. Fusion 47 (2007) 762.
[146] N. Asakura et al., Phys. Rev. Lett. 84 (2000) 3093.
[147] J.A. Boedo et al., Phys. Plasmas 5 (1998) 4305.
[148] J.A. Boedo et al, submitted to Phys. Plasmas. 2008.
[149] B. LaBombard et al., Phys. Plasmas 12 (2005) 056111.
[150] V. Naulin, J. Nucl. Mater. 363-365 (2007) 24-31.
[151] G.D. Porter, R. Isler, J. Boedo, Phys. Plasmas 7 (2000) 3663.

[152] G.D. Porter et al., J. Nucl. Mater. 313–316 (2003) 1085.

[153] R. Pitts et al., J. Nucl. Mater. 337–339 (2005) 146.

[154] A.V. Chankin et al., J. Nucl. Mater. 290–293 (2001) 518.

[155] V.A. Rozhansky et al., Nucl. Fusion 41 (2001) 387.

[156] X. Bonnin et al., J. Nucl. Mater. 337–339 (2005) 301.

[157] G.S. Kirnev et al., J. Nucl. Mater. 337–339 (2005) 271.

[158] T.D. Rognlien et al., J. Nucl. Mater. 337–339 (2005) 327.

[159] A.Yu. Pigarov, S.I. Krasheninnikov, B. LaBombard, 10th Intl. Workshop on Plasma Edge Theory in Fusion Devices, 17–19 October 2005, Julich.

[160] A.V. Chankin, P.C. Stangeby, Nucl. Fusion 41 (2001) 421.

[161] C. Hidalgo et al., J. Nucl. Mater. 313–316 (2003) 863.

[162] A.V. Chankin et al, private communication.

[163] B. LaBombard et al., Phys. Plasmas 15 (2008) 056106.

## ACKNOWLEDGMENT

This work supported by the US Department of Energy under DE-FG07-ER54917 and DE-FC02-04ER54698. We acknowledge help by D.L. Rudakov, B. LaBombard, R. Pitts, W. Fundamenski and A. Loarte. T. Leonard, M. Umanski and J. Myra.